# Comparative studies of optical absorption, photoluminescence and EPR spectra of PbMnI$_2$ bulk layers and nanocrystals

**A.I. Savchuk[1], I.D. Stolyarchuk[1], O. A. Savchuk[1], O.A. Shporta[1], I. Stefaniuk[2], I. Rogalska[2], E. Sheregii[2]**

[1]*Department of Physics of Semiconductors and Nanostructures, Chernivtsi National University,*
*2, Kotsiubynsky str., 58012 Chernivtsi, Ukraine, e-mail: a.savchuk@chnu.edu.ua*
[2]*Institute of Physics, University of Rzeszow, 16a Rejtana Street, 35959 Rzeszow, Poland*

**Abstract.** We report a study of the layered diluted magnetic semiconductor (DMS) $Pb_{1-x}Mn_xI_2$ in 3D bulk layers and nanocrystal form by using optical absorption, photoluminescence and electron paramagnetic resonance (EPR). The samples of the bulk $Pb_{1-x}Mn_xI_2$ crystals with $x$ lying within the range 0 to 0.15 were grown using the Bridgman-Stockbarger technique. The composite nanostructures containing DMS nanocrystals of $Pb_{1-x}Mn_xI_2$ were prepared by cooling the boiling saturated aqueous solution to room temperature. The exciton structure of the absorption spectra of nanoparticles exhibits blue shift due to the quantum confinement effect. In photoluminescence spectra of nanocrystals, two main peaks were revealed, which are attributed to the band-edge transitions and defect states. The EPR spectra for bulk layers and nanocrystals consist of an intense broad line and several weak narrow lines that correspond to hyperfine spectra of $Mn^{2+}$ ions.

**Keywords:** PbMnI$_2$, diluted magnetic semiconductor, nanoparticle, nanocrystal, optical absorption.

## 1. Introduction

In the recent decade, after the discovery of grafene and its unique properties [1, 2], interest to other materials with layered structures has significantly increased. Among them, lead iodide (PbI$_2$) is an intrinsic wide band gap semiconductor ($E_g$ = 2.3…2.55 eV) having high molecular weight and high resistivity. This material is an excellent and interesting candidate for high efficiency room temperature radiation detectors operating in the medium energy range. They can be widely applied in medicine, monitoring ecology, nondestructive defectoscopy and X-ray and gamma spectroscopy [3-6]. As a high-anisotropic semiconductor, PbI$_2$ has a type of layered structure, with a repeating unit of hexagonal close packed layer of Pb$^{2+}$ sandwiched between two layers of I$^-$ in the crystal.

Recently, a number of research works have been reported on the synthesis of the low-dimensional structures of PbI$_2$ by chemical and physical methods with different shapes. For example, colloidal [7-9], sol-gel [10, 11], reverse micells [12], hydrothermal techniques [13, 14] and so on were employed for growth of the PbI$_2$ nanostructures in the form of nanoplates, nanodisks, nanorods, nanodots, nanobelts and nanobelts bundles. All these structures demonstrate anisotropy of properties and a strong exciton confinement.

PbI$_2$ single crystals doped with transition metal (TM) elements (Mn, Fe, Co, etc) possessing the unfilled 3$d$-shell are of interest for the development of new materials – layered diluted magnetic semiconductors (LDMSs) [15, 16]. The main characteristics of these materials are associated with exhibition of strong $sp$-$d$ spin-exchange interaction between band carriers and magnetic ions. All materials having natural layered structures are expected to facilitate the growth of zero dimensional quantum-confined nanostructures due to their anisotropy along the directions parallel and perpendicular to the $C$ axis. Basic investigations of these materials are related to optical and magneto-optical

properties of bulk crystals, for example, $Pb_{1-x}Mn_xI_2$ [17-19], and related nanoparticles are insufficiently studied as yet [16, 20].

Electron paramagnetic resonance (EPR) is found to be a convenient technique because of variations of the EPR linewidth and possibility to investigate the spin-spin interactions in crystals. The line shape as a function of magnetic ion concentrations and temperature provides information about the dynamics of the spin system.

In this work, we report on absorption, photoluminescence (PL) and EPR studies of $Pb_{1-x}Mn_xI_2$ bulk layers and nanocrystals.

## 2. Experimental

### 2.1. Sample preparation

The samples of the $Pb_{1-x}Mn_xI_2$ layered crystals with $x$ lying within the range 0 to 0.15 were grown using the Bridgman-Stockbarger technique. The obtained 2H-polytype single crystal samples are characterized by clear-layered structures and very thin layers with the thickness up to 100 nm can be prepared by using the so-called "scotch tape method". Nanoparticles of $Pb_{1-x}Mn_xI_2$ with $x$ from the above range were prepared by embedding them into polyvinylalcohol (PVA) matrix using cooling the boiling saturated aqueous $Pb_{1-x}Mn_xI_2$ solution to room temperature [10, 21]. Originally, monocrystalline or polycrystalline $Pb_{1-x}Mn_xI_2$ was crushed to powder using the ball milling technique. The powder was dissolved in deionized water heated to 100 ℃. We added also PVA to solution for stabilization of the semiconductor particles. The mixture was cooled then to room temperature and kept at this temperature for 48 h. Polymer films with incorporated semiconductor particles that were produced in such a way were stable for a long period of time. Their stability was even higher than monocrystalline material. In the previous work [20], we have studied nanoparticles using TEM in the direction perpendicular to the $C$ axis. In this work, the scanning electron examination in the direction parallel to the $C$ axis was performed with a high-resolution field emission scanning electron microscope (FE SEM) Hitachi 5500 in order to confirm the platelet-like shape of nanocrystals (Fig. 1). The cross-section of the PVA film with nanoparticles of $Pb_{1-x}Mn_xI_2$ was prepared by the focused ion beam (FIB) technique.

### 2.2. Measurements

The absorption and photoluminescence spectra were recorded using the UV-Vis spectrometer based on the diffraction monochromator MDR-23 (LOMO) at temperatures 4.2 to 300 K. Excitation of photoluminescence was carried out using a He-Cd laser operating at the wavelength 325 nm and power close to 10 mW. For comparison, the measurements were performed separately for polymer films without nanoparticles, composite films and single crystal layers. For EPR measurements, the X-band microwave frequency
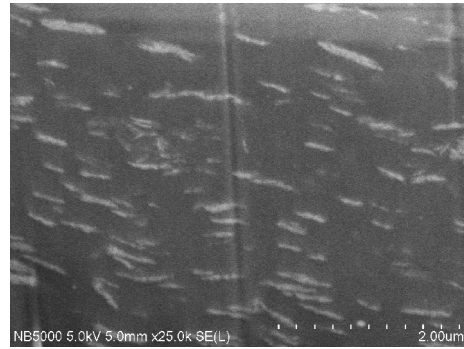


**Fig. 1.** SEM images of the $PbMnI_2$ nanoparticles embedded into PVA polymer matrix. The C axis of nanocrystals is parallel to the plane of photo.

(9.3 GHz, magnetic field modulation 100 kHz, power 5 mW, modulation amplitude 0.05 mT) in the Bruker Elexsys 580 FT/CW Q and X-band spectrometer was used. Temperature measurements were made using the variable temperature nitrogen controller (Bruker ER4131VT) and the Bruker Elexsys software, which enabled our investigations within the temperature range 90 to 370 K. The samples were cut in the shape of a circle of the radius about 1.5 mm.

## 3. Results and discussion

The exciton absorption spectrum of thin layers of pure $PbI_2$ consists of three lines with $n = 1, 2$ and 3. In the case of solid solutions of $Pb_{1-x}Mn_xI_2$ with $x \leq 0.01$, exciton structures reduced to two lines with $n = 1, 2$ and contained only the main exciton band $n = 1$, when $x > 0.01$. In addition, with an increase of Mn content main exciton band is strongly broadened and shifted towards shorter wavelengths. Similar behavior is observed in the exciton reflection spectra of bulk layers of $Pb_{1-x}Mn_xI_2$ (Fig. 2). With increasing the manganese content, we observed high-energy shift of the exciton structure $n = 1$, its broadening and disappearance of the $n = 2$ and $n = 3$ exciton excited states in $PbI_2$. The exciton structure in the studied samples is well explained in terms of the cationic exciton model [22]. In accordance with this model, the main peak is associated with the optical transition between $A_4^+$ valence band and $A_4^-$ conduction band. Experimental data on the exciton energy position at different Mn mole fractions $x$ show a linear relationship, and they are in good agreement with the empirical expression for the $1s$ exciton peak at the temperature $T = 4.2$ K:

$$E_{ex}(x) = [2.5 + (1.25 \pm 0.05)\,x]\ \text{eV}. \qquad (1)$$

With decreasing dimensionality of the system to nanocrystals, one can see changes in absorption spectra. The exciton structure of the absorption spectra of nanoparticles exhibits a blue shift due to the quantum confinement effect. With decreasing temperature for

nanocrystals embedded into PVA matrix, we also observed only one broad band shifted to the short-wave side (Fig. 3). Similar deviation has been reported even for the exciton energies in the two- and three-layer nanoparticles of PbI$_2$ into E-MAA copolymer [23, 24]. Analyzing these spectra and using the quantum confinement model based on the effective-mass approximation, it is possible to estimate the thickness of these nanocrystals using the expression:

$$E = E_b + \frac{\pi^2 h^2 n^2}{2M L_z^2} ,  \qquad (2)$$

where $E_b$ is the exciton formation energy in the material (bulk), and $M$ is the exciton translation mass, $L_z$ is the width of the potential well, and $n$ is the quantum number of loops of the standing wave. The performed calculations according to Eq. (2) suggest that the thickness $L_z$ of nanoparticles is equal to 0.7 nm (unit layer).

Fig. 4 depicts the low-temperature PL spectra for bulk layers of Pb$_{1-x}$Mn$_x$I$_2$ at band-to-band excitation. For pure PbI$_2$, the PL spectrum consists of an intense emission band corresponding to the exciton-impurity complex of I and two weak bands A$_T$ and A$_D$ related with the emission of polaritons of the upper and lower branches, respectively. In Pb$_{1-x}$Mn$_x$I$_2$ layers with $x = 0.01$, we observed two emission bands I and I$_L$ and polariton band like that in pure PbI$_2$. With increase of the Mn content, the PL spectra shifted to the high energy region with disappearance of the I, A$_T$ and A$_D$ bands, and only one broad emission band was observed. This broad emission band demonstrates a small asymmetry at the low-energy side. On the other hand, with increasing the temperature for the high-energy tail of this band its broadening is observed. This behavior suggests that the broad emission band is associated with the localized excitons. The localized exciton states may be induced by potential fluctuations caused by imperfections in the crystal. These imperfections of the crystal lattice occur in the samples as a consequence of substitution of lead atoms (ion radius 1.26 Å) in the cation sublattice by manganese atoms (ion radius 0.91 Å).
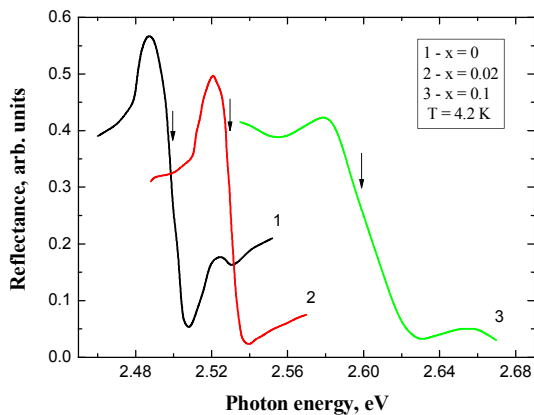


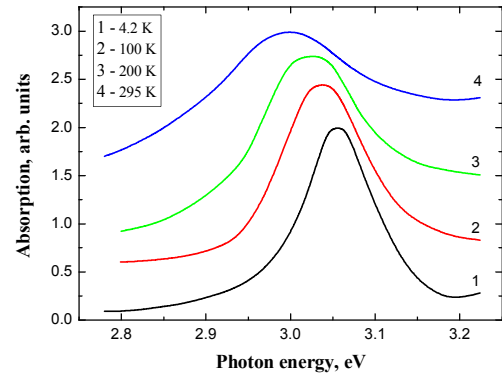**Fig. 3.** Absorption spectra of Pb$_{0.97}$Mn$_{0.03}$I$_2$ nanocrystals embedded into PVA matrix at different temperatures.



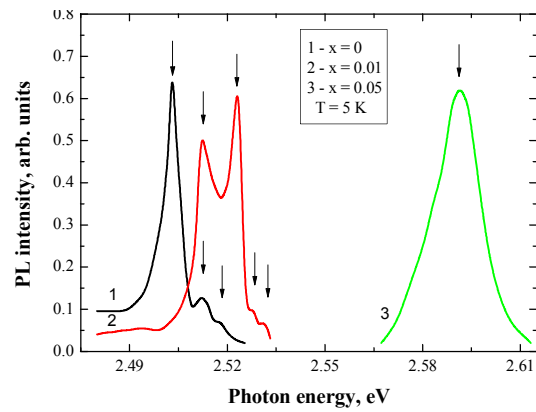**Fig. 4.** Low-temperature photoluminescence spectra of bulk layers Pb$_{1-x}$Mn$_x$I$_2$ with a different Mn content.

The room temperature photoluminescence spectrum for nanocrystals of Pb$_{1-x}$Mn$_x$I$_2$ in PVA matrices is shown in Fig. 5. The two peaks are observed in all the samples with a different Mn content. The high-energy emission peaks can be attributed to the exciton transitions. The energy position of this band is shifted to higher photon energies with increasing the Mn content in accordance with reducing the band gap. The energy position of the low-energy photoluminescence peak is around 2.35…2.38 eV. With increasing the manganese content, we observed increase in the intensity of this band and its broadening. However, the energy position of the PL peak remains the same up to $x \le 0.03$. On the other hand, with further increasing the TM component ($x > 0.03$) we observed a small blue shift of the low-energy band of spectrum. This emission band is associated with a different defect states. E. Lifshitz et al. [10, 25] observed an emission band in PL spectra for platelet-like nanocrystals PbI$_2$ in this energy region and identified this peak with donor and acceptor sites at the interior part of the nanoparticles. N. Preda et al. [26] observed an emission band with simple energy position in PL spectra for micrometric crystalline powder of PbI$_2$ obtained by mechanical crumbling of bulk crystals. They associated this peak with the presence of Pb$^{2+}$ ions
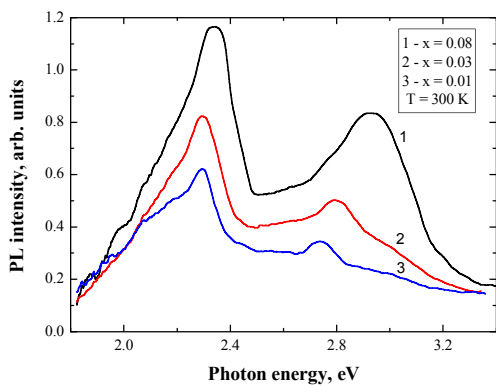


**Fig. 2.** Low-temperature exciton reflection spectra of bulk layers of Pb$_{1-x}$Mn$_x$I$_2$ with a different Mn content.

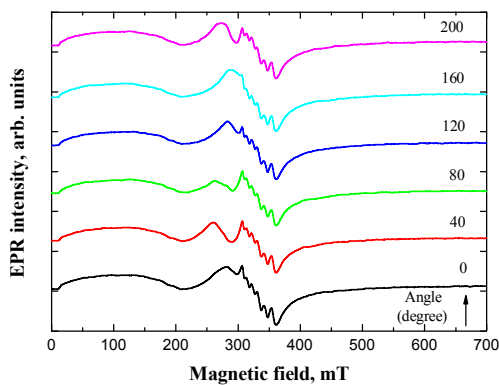**Fig. 5.** Room temperature photoluminescence spectra of $Pb_{1-x}Mn_xI_2$ nanocrystals in PVA matrix.



**Fig. 6.** Room temperature EPR spectra for $Pb_{0.92}Mn_{0.08}I_2$ nanocrystals for the axis of rotation in the plane of the sample at different angles.

usually produced near dislocations and cleavage defects in bulk crystals. S.E. Derenzo et al. [27] studied $PbI_2$ crystals with different impurities and associated a similar emission band in PL spectra with recombination between shallow donors and acceptors.

Electron paramagnetic resonance spectra for bulk layers of $Pb_{1-x}Mn_xI_2$ and nanocrystals were investigated in the X-band [28]. The EPR spectrum that we are observed is typical for $Mn^{2+}$ ions in polycrystalline samples. The basic spectrum consists of typical hyperfine structure (six lines for 5/2 nuclear spin) and transition between spin levels $m_s = -1/2$ to $m_s = +1/2$ superposed on the wide line. The wide line that is observed in EPR spectrum consists of 4 broaden lines for $Mn^{2+}$, which are described for bulk materials in [29, 30] and nanocrystals [31, 32] as related with transitions between spin levels $m_s = -5/2$ to $m_s = -3/2$, $m_s = -3/2$ to $m_s = -1/2$, $m_s = +1/2$ to $m_s = +3/2$, and $m_s = +3/2$ to $m_s = +3/2$. Simultaneously, for the samples with a higher value of $x$, such as $x > 0.01$ for bulk crystals and $x > 0.08$ for nanocrystals, a hyperfine structure is completely quenched, and only a broad signal is observed. The values of effective spectroscopic $g_{eff} = 1.995$ agrees very well with that presented in the

literature [33]. Besides, for nanoparticles with the manganese content $x \leq 0.08$ and bulk layers with $x \leq 0.01$, we also observed other resonance line with anisotropy in the angular dependence (Fig. 6). The character of angular and temperature dependences suggests that this resonance line is related with Mn atoms substituting lead atoms inside the crystal layer [34]. Full interpretation of this EPR line requires further researches.

## 4. Conclusions

In conclusion, the optical absorption, photoluminescence and EPR spectra for bulk layers and nanocrystals of $Pb_{1-x}Mn_xI_2$ have been studied. The exciton structure in absorption spectra of nanocrystals is shifted to shorter wavelengths as compared with that of bulk layers due to the quantum confinement effect. The broad emission band in photoluminescence spectra of $Pb_{1-x}Mn_xI_2$ bulk layers is associated with localized states of excitons. In PL spectra of nanocrystals, two peaks have been observed, which are attributed to the band-edge transitions and defect states. The EPR spectra for the investigated samples consist of an intense broad line and several weak narrow lines that correspond to hyperfine spectra of $Mn^{2+}$ ions. As the manganese content increases, the hyperfine structure transforms to one broad line. The values of effective spectroscopic $g_{eff} = 1.995$ parameters of hyperfine structure A and the peak-to-peak line width of the resonance line $H_{pp}$ have been obtained for the hyperfine structure.

*References*

1. K.S. Novoselov, A.K. Geim, S.V. Morozov, D. Jiang, Y. Zhang, S.V. Dubonos, I.V. Grigorieva, and A.A. Firsov, Electric field effect in atomically thin carbon films // *Science,* **306**, p. 666-669 (2004).
2. A.K. Geim, K.S. Novoselov, The rise of graphene // *Nat. Mater.* **6**, p. 183-191 (2007).
3. Y.-C. Chang and R.B. James, Phonon dispersion and polar-optical scattering in 2H $PbI_2$ // *Phys. Rev. B,* **55**, p. 8219-8225 (1997).
4. M. Matuchova, K. Zdansky, J. Zavadil, J. Tonn, Mousa M. Abdul-Gader Jafar, A.N. Danilewsky, A. Croll, J. Maixner, Influence of doping and non-stoichiometry on the quality of lead iodide for use in X-ray detection // *J. Cryst. Growth,* **312**, p. 1233-1239 (2010).
5. M. Matuchova, K. Zdansky, J. Zavadil, Lead iodide crystals prepared under stoichiometric and nonstoichiometric conditions // *Mater. Sci. Eng. B,* **165**, p. 60-63 (2009).

6.  A.M. Caldeira Filho, M. Mulato, Characterization of thermally evaporated lead iodide films aimed for the detection of X-rays // *Nucl. Instrum. and Meth. A*, **636**, p. 82-86 (2011).

7.  C.J. Sandroff, D.M. Hwang, W.M. Chung, Carrier confinement and special crystallite dimensions in layered semiconductor colloids // *Phys. Rev. B*, **33**, p. 5953-5955 (1986).

8.  J.P. Ponpon, M. Amann, Properties of solution grown $PbI_2$ layers embedded in PVA // *Cryst. Res. Technol*. **42**, p. 253-259 (2007).

9.  E.M.S. dos Santos, L.S. Pereira, G.J.-F. Demets, Quantum confinement in $PbI_2$ nanodisks prepared with cucurbit[7]uril // *J. Braz. Chem. Soc*. **22**, p. 1595-1600 (2011).

10. E. Lifshitz, M. Yassen, L. Bykov, I. Dag, Continuous photoluminescence, time resolved photoluminescence and optically detected magnetic resonance measurements of $PbI_2$, nanometer-sized particles, embedded in $SiO_2$, films // *J. Lumin*.**70**, p. 421-434 (1996).

11. Yu. A. Barnakov, S. Ito, I. Dmitruk, S. Tsunekawa, A. Kasuya, Production and optical study of $PbI_2$ nanorod-like particles // *Scripta Materiala,* **45**, p. 273-277 (2001).

12. G.K. Kasi, N.R. Dollahon, T.S. Ahmadi, Fabrication and characterization of solid $PbI_2$ nanocrystals // *J. Phys. D: Appl. Phys*. **40**, p. 1778-1783 (2007).

13. G. Zhu, M. Hojamberdiev, P. Liu, J. Peng, J. Zhou, X. Bian, X. Huang, The effects of synthesis parameters on the formation of $PbI_2$ particles under DTAB-assisted hydrothermal process // *Mat. Chem. Phys*. **131**, p. 64-71 (2011).

14. G. Zhu, P. Liu, M. Hojamberdiev, J. Zhou, X. Huang, B. Feng, R. Yang, Controllable synthesis of $PbI_2$ nanocrystals via a surfactant-assisted hydrothermal route // *Appl. Phys. A*, **98**, p. 299-304 (2010).

15. P.I. Nikitin and A.I. Savchuk, The Faraday effect in semimagnetic semiconductors // *Sov. Phys. Usp*. **33**, p. 974-989 (1990).

16. P.I. Nikitin, A.I. Savchuk, S.V. Medynskiy, and I.D. Stolyarchuk, Optical absorption studies on nano-crystals of semimagnetic semiconductor $PbMnI_2$ // *Cryst. Res. Technol*. **31**, p. 623-626 (1996).

17. O. Rybak, I.V. Blonskii, Ya.M. Bilui, Yu. Lun, M. Makowska-Janusik, J. Kasperczyk, J. Berdowski, I.V. Kityk, and B. Sahraoui, Luminescent spectra of $PbI_2$ single crystals doped by 3d-metal impurities // *J. Lumin*.**79**, p. 257-267 (1998).

18. I.V. Blonskii, J.D. Nabytovych, Yu.O. Loon, and O.V. Rybak, Peculiarities of manifestation of different forms of structure disordering in the exciton spectra of the $PbI_2$ // *Phys. Status Solidi* (*a*), **174**, p. 353-360 (1999).

19. I.M. Kravchuk, S.S. Novosad, and I.S. Novosad, Luminescence from Mn-doped $PbI_2$ crystals // *Techn. Phys*. **46**, p. 262-265 (2001).

20. A.I. Savchuk, V.I. Fediv, Ye.O. Kandyba, T.A. Savchuk, I.D. Stolyarchuk, and P.I. Nikitin, Platelet-shaped nanoparticles of $PbI_2$ and $PbMnI_2$ embedded in polymer matrix // *Mater. Sci. Eng. C,* **19**, p. 59-62 (2002).

21. M.V. Artemyev, Yu.P. Rakovich, G.P. Yablonski, Effect of dc electric field on photoluminescence from quantum-confined $PbI_2$ nanocrystals // *J. Cryst. Growth,* **171**, p. 447-452 (1997).

22. Y. Nagamune, S. Takeyama, M. Miura, Exciton spectra and anisotropic Zeeman effect in $PbI_2$ at high magnetic fields up to 40 T // *Phys. Rev. B,* **43**, p. 12401-12405 (1991).

23. T. Goto, S. Saito, M.Tanaka, Size quantization of excitons in $PbI_2$ microcrystallites // *Solid State Communs*. **80**, p. 331-334 (1991).

24. S. Saito, T. Goto, Spatial-confinement effect on phonons and excitons in $PbI_2$ microcrystallites // *Phys. Rev. B,* **52**, p. 5929-5934 (1995).

25. E. Lifshitz, L. Bykov, M. Yassen, Z. Chen-Esterlit, The investigation of donor and acceptor states in nanoparticles of the layered semiconductor $PbI_2$ // *Chem. Phys. Lett*. **273**, p. 381-388 (1997).

26. N. Preda, L. Mihut, M. Baibarac, I. Baltog, S. Lefrant, Distinctive signature in the Raman and photoluminescence spectra of intercalated $PbI_2$ // *J. Phys.: Condens. Matter,* **18**, p. 8899-8912 (2006).

27. S.E. Derenzo, E. Bourret-Courchesne, Z. Yan, G. Bizarri, A. Canning, G. Zhang, Experimental and theoretical studies of donor-acceptor scintillation from $PbI_2$ // *J. Lumin*. **134**, p. 28-34 (2013).

28. A.I. Savchuk, I.D. Stolyarchuk, I. Stefaniuk, I. Rogalska, E. Sheregii, V.V. Makoviy, O.A. Shporta, Electron paramagnetic resonance spectra of $PbMnI_2$ bulk crystals and nanocrystals // *J. Mag. Magn. Mat*. **345**, p. 134-137 (2013).

29. C.J. Bender and L.J. Berliner (eds.), *Computational and Instrumental Methods in EPR*. Springer, New York, 2006.

30. A. Angerhofer, E. W. Moomaw, I. Garcia-Rubio, A. Ozarowski, J. Krzystek, R. T. Weber, and N. G. J. Richards, Multifrequency EPR studies on the Mn(II) centers of oxalate decarboxylase // *J. Phys. Chem. B,* **111**, p. 5043-5046 (2007).

31. M. Qazzaz, G. Yang, S.H. Xin, L. Montes, H. Luo, and J.K. Furdyna, Electron paramagnetic resonance of $Mn^{2+}$ in strained-layer semiconductor superlattices // *Solid State Communs*. **96**, p. 405-409 (1995).

32. Z. Wang, W. Zheng, J. van Tol, N.S. Dalal, and G.F. Strouse // *Chem. Phys. Lett*. **524**, p. 73-77 (2012).

33. F.V. Motsnyi, V.G. Dorogan, Z.D. Kovalyuk, S.M. Okulov, and A.M. Yaremko, Spectroscopic studies of $2H-PbI_2(Mn)$ layered crystals // *Phys. Status Solidi* (*b*), **242**, p. 2427-2432 (2005).

34. V.V. Slyn'ko, A.G. Khandozhko, Z.D. Kovalyuk, V.E. Slyn'ko, A.V. Zaslonkin, M. Arciszewska, and W. Dobrowolski, Ferromagnetic states in the $In_{1-x}Mn_xSe$ layered crystal // *Phys. Rev. B*, **71**, 245301 (2005).